Title	Conformation, hydration, and ligand exchange process of ruthenium nitrosyl complexes in aqueous solution; Free-energy calculations by a combination of molecular-orbital theories and different solvent models
Author(s)	Kido Kentaro, Kaneko Masashi
Citation	Journal of Computational Chemistry, 44(4), p.546-558
Text Version	Accepted Manuscript
URL	https://jopss.jaea.go.jp/search/servlet/search?5075786
DOI	https://doi.org/10.1002/jcc.27021
Right	This is the peer reviewed version of the following article: Kido, K., Kaneko, M., J. Comput. Chem. 2023, 44(4), 546. https://doi.org/10.1002/jcc.27021, which has been published in final form at https://doi.org/10.1002/jcc.27021. This article may be used for non-commercial purposes in accordance with Wiley Terms and Conditions for Use of Self-Archived Versions. This article may not be enhanced, enriched or otherwise transformed into a derivative work, without express permission from Wiley or by statutory rights under applicable legislation. Copyright notices must not be removed, obscured or modified. The article must be linked to Wiley's version of record on Wiley Online Library and any embedding, framing or otherwise making available the article or pages thereof by third parties from platforms, services and websites other than Wiley Online Library must be prohibited.

Journal of COMPUTATIONAL CHEMISTRY WWW.C-CHEM.ORG FULL PAPER

Conformation, hydration and ligand exchange process of ruthenium nitrosyl complexes in aqueous solution: Free-energy calculations by a combination of MO theories and different solvent models

Kentaro Kido[1] and Masashi Kaneko[2]

Correspondence to: Kentaro Kido (E-mail: kido.kentaro@jaea.go.jp) and Masashi Kaneko (E-mail: kaneko.masashi@jaea.go.jp)

[1] *Kentaro Kido*
Nuclear Safety Research Center, Japan Atomic Energy Agency, 2-4 Shirane, Shirakata, Tokai-mura, Naka-gun, Ibaraki, Japan, 319-1195.
[2] Masashi Kaneko
Nuclear Science and Engineering Center, Japan Atomic Energy Agency, 2-4, Shirane, Shirakata, Tokai-mura, Naka-gun, Ibaraki, Japan, 319-1195.

ABSTRACT

Distribution of solvent molecules near transition-metal complex is key information to comprehend the functionality, reactivity and so on. However, polarizable continuum solvent models still are the standard and conventional partner of molecular-orbital (MO) calculations in the solution system including transition-metal complex. In this study, we investigate the conformation, hydration and ligand substitution reaction between NO_2^- and H_2O in aqueous solution for $[Ru(NO)(OH)(NO_2)_4]^{2-}$ (**A**), $[Ru(NO)(OH)(NO_2)_3(ONO)]^{2-}$ (**B**) and $[Ru(NO)(OH)(NO_2)_3(H_2O)]^-$ (**C**) using a combination method of MO theories and a state-of-the-art molecular solvation technique (NI-MC-MOZ-SCF). A dominant species is found in the complex **B** conformers and, as expected, different between the solvent models, which reveals that molecular solvation beyond continuum media treatment are required for a reliable description of solvation near transition-metal complex. In the stability constant evaluation of ligand substitution reaction, an assumption that considers the direct association between the dissociated NO_2^- and complex **C** is useful to obtain a reliable stability constant.

Introduction

A great number of ruthenium nitrosyl complexes have been extensively developed from industrial and physiological interests, for example, as a catalyst[1–3], antihypertensive agent, anti-cancer drug[4–6] and so on. Very recently, Liu et al. have reported that the complex $[Ru(NO)(Hbdalk)(pic)_2]^{2-}$, where H_2bdalk and pic denote 2,2′-[2,2′-bipyridine]-6,6′-diyl and 4-picoline, respectively, shows a catalytic capability for water oxidation to oxygen molecule[3]. The electronic state of Ru-NO is non-trivial due to the complicated dependency on the ligand field[7]. Continuous efforts to understand and characterize the bond nature still have been made, for example, the theoretical study using a large-scale complete-active space self-consistent field (CASSCF) of the *trans*-$[RuCl_4(NO)(1H\text{-indazole})]$-complex (very similar to the anti-cancer drug, KP1019[8, 9]) reports that the Ru^{III}-NO^0 oxidation state has a larger contribution than Ru^{II}-NO^+ in the multi-configurational character of Ru-NO moiety for both the singlet and triplet states.[10]

The complex family $[Ru(NO)(NO_3)_i(NO_2)_j(OH)_k(H_2O)_l]^{(3-i-j-k)+}$ (**1**$_{ijkl}$)[11–16] is yielded in a concentrated nitric acid aqueous solution used in several industrial processes. In

the separation of noble metals, the extracting agent has been designed to efficiently recover ruthenium from the complex[17–24]. The liquid waste after nuclear fuel reprocessing, which is called high-level liquid waste (HLLW), contains the complex family as well as various transition-metal complexes. Isotopes of the transition metal including ruthenium are highly radioactive and constantly generates the decay heat. If the heat is not properly removed, ruthenium tetroxide (RuO_4) is produced from complex $\mathbf{1}_{ijkl}$ by being continuously heated and can be transferred to the environment due to the high volatility, which is known as the representative risk in a severe accident of reprocessing plant [25–30]. Using ^{15}N NMR spectroscopy, Kabin et al. have studied $[Ru(NO)(NO_2)_4(OH)]^{2-}$ (complex **A**, Scheme 1) and the derivatives by ligand exchange reactions in nitric acid aqueous solution (the concentration range is 0-3.3 mol/L)[31, 32]. However, it is difficult to access to the conformation structure in solution and solvation properties by using experimental techniques. So, despite of requirements of the risk assessment, very limited information is available to specify *i*, *j*, *k* and *l* in complex $\mathbf{1}_{ijkl}$ depending on the nitric acid concentration[33]. This makes a systematic understanding the reaction pathway from complex $\mathbf{1}_{ijkl}$ to RuO_4 impossible.

The goal of this study is to predict the distribution of conformers of $[Ru(NO)(OH)(NO_2)_3(ONO)]^{2-}$ (complex **B**) and $[Ru(NO)(OH)(NO_2)_3(H_2O)]^{-}$ (complex **C**) in aqueous solution and the stability constant for the nitro(NO_2)-aqua or nitrito(ONO)-aqua ligand exchange process observed in the chemical equilibria among complex **A**, **B** and **C** based on a free-energy calculation with a quantum mechanics/molecular mechanics (QM/MM)[34, 35]-type approach. The conformation distribution provides key information to unravel the ligand-exchange process and RuO_4 production mechanism at molecular level. For example, in the Grubbs-type ruthenium complexes, the catalytic activity is controlled by ligand orientations[36].

A lot of theoretical studies on ruthenium nitrosyl complexes using *ab initio* molecular-orbital (MO) and density functional theories (DFTs) have been devoted so far to the NO bond nature and photochemical NO dissociation processes from interests as a NO donor[10, 37–49]. In the studies, solvation effects are usually incorporated with various formalisms of polarizable continuum model (PCM)[50, 51]. To take effects of hydrogen bonds into account, a solvation model is also employed to involve several discrete water molecules around the metal complex as the first solvation shell in the PCM solvent[42]. But, an explicit description of solvent is required for the present system to obtain a reliable conformation distribution because the hydroxyl, nitro and nitrite ligands form the strong hydrogen bond with solvent water. For ruthenium nitrosyl complexes in solution, few classical Monte Carlo simulations[42, 49] and QM/MM studies have been reported so far to obtain the solvation properties due to the huge computational cost.

To overcome it, we employ multi-center molecular Ornstein-Zernike self-consistent field (MC-MOZ-SCF)[52, 53] method, which is a combination between MO theories (solute) and MC-MOZ[54–56] (solvent). MC-MOZ is an explicit solvent model based on the integral equation theory for molecular liquids[57–60] and describes the solvent as a density distribution function. As shown later, the method also provides the three-dimensional (3D) solvation structure near solute. Furthermore, a free energy of solute is readily evaluated by the analytical expression of the distribution function obtained by solving the MC-MOZ equation[52, 53, 61, 62]. Thanks to it, compared with a free-energy calculation by conventional QM/MM using molecular simulation techniques, we can perform the procedure with a very low computational cost. Hence, we can choose a sophisticated method such as MP2 and CCSD(T) in the QM region.

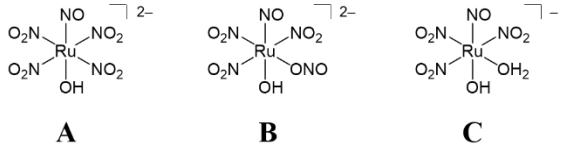

Scheme 1. Structural formulas of complexes **A**, **B** and **C**.

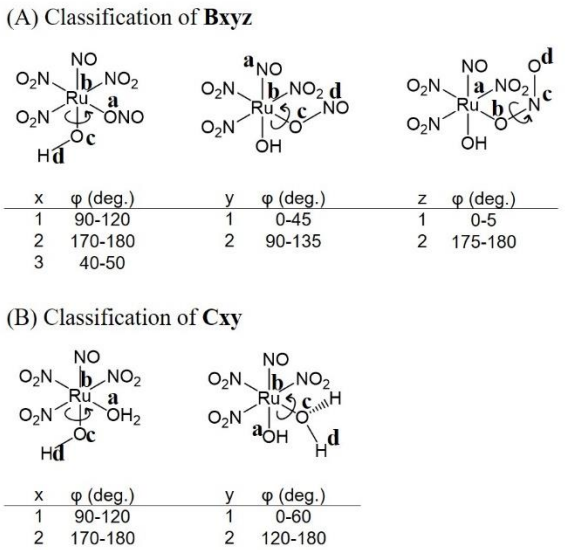

Scheme 2. Classification by dihedral angle (ϕ) consisting of atoms a-b-c-d for conformers Bxyz and Cxy.

Table 1. Basis set used in this study.

Atom	BS-I	BS-II
Ru	LanL2DZ	LanL2TZ(f)
N		
O	aug-cc-pVDZ	aug-cc-pVTZ
H		

Previous studies show that the method provides an accurate solvation free energy (SFE) for small molecules and ions in several solvents[53, 63].

In this study, we select a non-iterative version of MC-MOZ-SCF method[53]. It provides a similar result to the original within an acceptable error in shorter computational time. For a comparison, PCM is also used for the solvation energy evaluation. For a comprehensive investigation of conformers of complex **B** and **C**, we construct the conformation with a systematic way, as shown later. By estimating the free energy in aqueous solution for each conformer and complex **A** with both solvent models, we calculate the conformer distribution and stability constant. They are compared with the experimental result and analyzed by an energy decomposition in order to investigate a level of MO theory and solvent model to obtain a reliable value.

Theory and computational details

To choose a proper method for geometry optimization in a comparison of the X-ray crystal structure, complex **A** was optimized in gas phase by BP86[64, 65], CAM-B3LYP[66], M06[67] and TPSSh[68, 69] with BS-I. Based on the result, in aqueous solution, using Gaussian 16 (G16C01)[70], all the geometry optimizations (complex **A**, **B**, **C**, **C11NO$_2$**, nitrite anion and water) were performed at CAM-B3LYP/BS-I level of theory with the PCM solvent (water). In energy evaluations, MP2, resolution of the identity (RI)-CCSD(T)[71] methods were employed with BS-II as well as various DFT functionals, *i.e.*, BP86, CAM-B3LYP, wB97X-D[72], M06, M06-L, TPSS and TPSSh. In MP2 and RI-CCSD(T), no frozen core is considered in the electron correlation energy calculation. In the RI-CCSD(T) calculation, aug-cc-pVTZ-RIFIT[73] was employed for all atoms as auxiliary basis set. As shown in Table 1, in BS-1, LanL2DZ[74] and aug-cc-pVDZ[75, 76] are used for ruthenium and other atoms, respectively. BS-II consists of LanL2TZ(f)[77, 78] for ruthenium and aug-cc-pVTZ[75, 76] for other atoms.

Conformation construction of complex B and C

Complex **B** and **C** were modelled by replacing one of the equatorial NO_2 ligands of complex **A** with ONO ligand and H_2O ligand, respectively. The coordination geometry of complex **A** based on the single crystal X-ray diffraction reported by Emel'yanov et al.[79] was used as their reference structure. In the modelling, the variation of replacing positions was not considered because preliminary demonstration regarding the replacing positions did not give meaning changes in the optimized geometries. Their possible

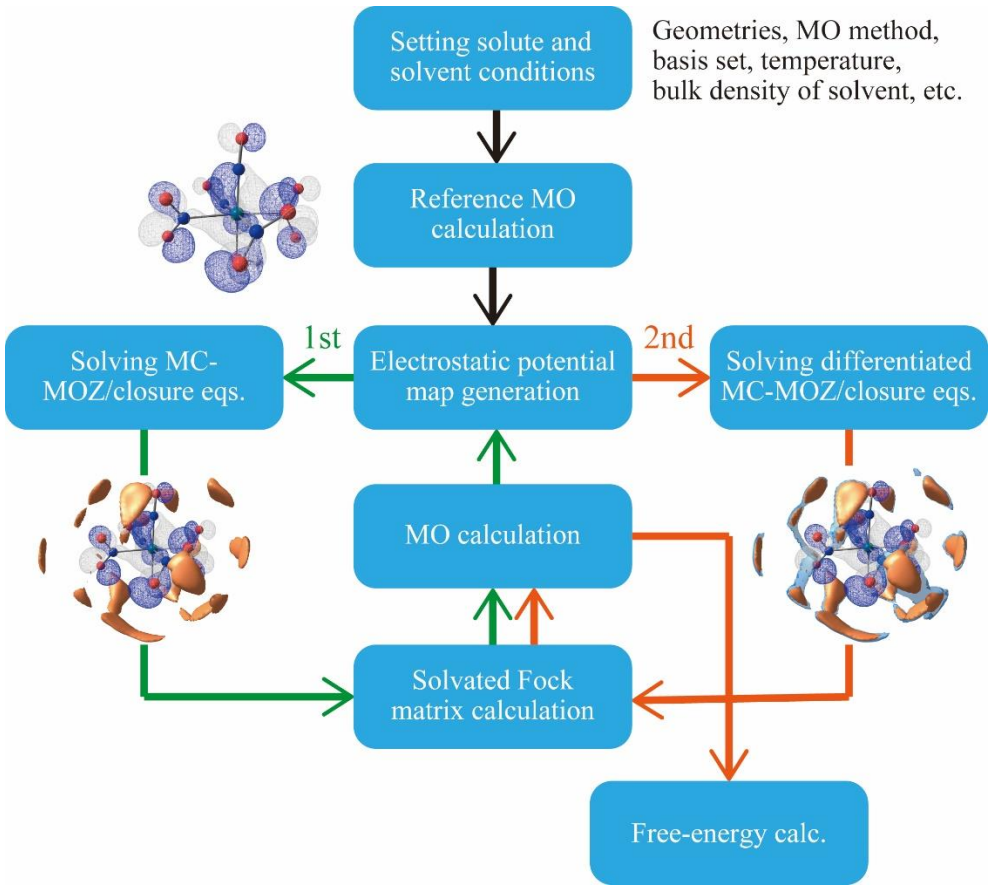

Scheme 3. A schematic procedure of NI-MC-MOZ-SCF.

conformers were constructed by considering the free rotation along Ru-ligand bond axes.

We defined the name of the conformers based on patterns of the bond rotation axes in conformation searching. In case of complex **B**, three patterns of the bond rotation axis, including Ru−OH, Ru−ONO and (Ru-)O−NO bonds, were considered, relating to the definitions of x, y and z, respectively, in **Bxyz**. The conformers of complex **C** were searched by the axis rotation of Ru−OH and Ru−OH_2 bonds, relating to the definitions of x and y, respectively, in **Cxy**. Scheme 2 describes a classification of conformers **Bxyz** and **Cxy**, in which x, y and z are determined by dihedral angle (ϕ) consisting of atoms **a-b-c-d**. The conformation searching resulted in nine conformers for complex **B** (**B111**, **B112**, **B121**, **B122**, **B211**, **B212**, **B221**, **B222** and **B321**) and four conformers for complex **C** (**C11**, **C12**, **C21** and **C22**). The ball-and-stick illustrations of the conformers were illustrated in Figure S1 and S2 in Supporting Information. The optimized Cartesian coordinates of all the conformers (given in Å unit) were also available in Supporting Information.

An explicit solvent model

A free energy of solute is expressed by

$$G = E^{\text{gas}} + E^{\text{reorg}} + G^{\text{sol}}, \qquad (1)$$

where E^{gas}, E^{reorg} and G^{sol} denote energy in gas phase, electronic reorganization energy and excess chemical potential, respectively. The zero-point energy is involved in the gas phase energy. E^{reorg} is defined by

$$E^{\text{reorg}} = \langle \Psi^{\text{sol}} | H^{\text{gas}} | \Psi^{\text{sol}} \rangle - \langle \Psi^{\text{gas}} | H^{\text{gas}} | \Psi^{\text{gas}} \rangle, \quad (2)$$

Table 2. LJ parameters used in this study.

Atom	σ / Å	ε / kcal mol^{-1}
Ru	2.6397	0.056
N (nitrosyl)	3.360	0.210
N (nitrito)	3.150	0.170
O (nitrosyl)	2.960	0.210
O (nitrito)	2.860	0.210
O (hydroxyl)	3.120	0.170
H	1.000	0.056

where H^{gas} represents the standard gas-phase Hamiltonian for solute molecule. Ψ^{sol} and Ψ^{gas} correspond to the solute wave function in solution and gas phases, respectively. In this study, the solvation free energy (SFE) is defined by the sum of electronic reorganization energy and excess chemical potential. The SFE of all the complexes, water and nitrite anion are computed by two approaches. One is PCM. The SFE by PCM is calculated using Gaussian 16 and solvent model density (SMD)[80] method is employed to obtain the non-electrostatic contribution.

The other is a non-iterative (NI-)MC-MOZ-SCF[53] method. The approach treats solvent as a density distribution based on the integral equation theory for molecular liquids. It enables us to calculate SFE and solvation structure with a high computational efficiency. If the reader is not familiar with the theory and method coupling with MO theories, please refer to the textbook[57, 58] and literature[59, 60]. Since details of the method were already published elsewhere[52, 53], here we briefly explain the procedure to evaluate the G^{sol} and hydration structure. Scheme 3 illustrates the procedure of NI-MC-MOZ-SCF. In the NI-MC-MOZ-SCF method, G^{sol} and the hydration structure $g_s(\mathbf{r})$ are expressed, as follows.

$$G^{\text{sol}} = G^{\text{sol},0} + \sum_{i,j} V_{ij}^0\, \delta D_{ij} + \frac{1}{2}\sum_{i,j,k,l} V_{ijkl}^1\, \delta D_{ij}\delta D_{kl}, \quad (3)$$

$$g_s(\mathbf{r}) = 1 + H_s^0(\mathbf{r}) + \sum_{i,j}\left(\frac{\partial H_s}{\partial D_{ij}}\right)^0 \delta D_{ij}\,, \quad (4)$$

where D_{ij} denotes the matrix element of density matrix and $\delta D_{ij} = D_{ij} - D_{ij}^0$. V_{ij}^0 and V_{ijkl}^1 are given by

$$V_{ij}^0 = -\int d\mathbf{r}\, A_{ij}(\mathbf{r}) \sum_s^{\text{solvent}} \rho_s q_s [H_s^0(\mathbf{r}) + 1]\,, \quad (3\text{-}1)$$

$$V_{ijkl}^1 = -\int d\mathbf{r}\, A_{ij}(\mathbf{r}) \sum_s^{\text{solvent}} \rho_s q_s \left(\frac{\partial H_s}{\partial D_{kl}}\right)^0, \quad (3\text{-}2)$$

respectively. Here, ρ_s and q_s denote the number density and point charge of solvent site s. $H_s(\mathbf{r})$ is the total correlation function. $A_{ij}(\mathbf{r})$ is a three-center one-electron integral and given by

$$A_{ij}(\mathbf{r}) = \int d\mathbf{r}' \frac{\chi_i(\mathbf{r})\chi_j(\mathbf{r}')}{|\mathbf{r} - \mathbf{r}'|}, \quad (5)$$

where $\chi_i(\mathbf{r})$ denotes a primitive gaussian of basis function. The superscript, 0, on the functions and valuables means the reference state of the NI-MC-MOZ-SCF method. In this study, the first iteration of reference interaction site model (RISM) SCF spatial electron density distribution (SEDD) approach[81] is employed as the reference state (Type C in Ref. [53]).

In this study, partial series expansion third order (PSE-3)[82] type closure was selected instead of hypernetted chain (HNC) closure because the coupled equation of MC-MOZ and HNC closure was not converged. Although this choice is different from the bulk solvent (HNC, shown later), as reported in Ref. 82, PSE-3 and HNC closures numerically provide nearly identical solvation properties. When MC-MOZ equation is coupled with PSE-3 type closure, $G^{\text{sol},0}$ can be written as

$$G^{\text{sol},0} = k_{\text{B}}T \sum_s^{\text{solvent}} \rho_s \int d\mathbf{r} \times [f_s^{\text{HNC}}(\mathbf{r}) - f_s^{\text{PSE-3}}(\mathbf{r})], \quad (3\text{-}3)$$

$$f_s^{\text{HNC}}(\mathbf{r}) = \frac{1}{2}[H_s^0(\mathbf{r})^2 - 2C_s^0(\mathbf{r}) - H_s^0(\mathbf{r})C_s^0(\mathbf{r})], \quad (6)$$

Table 3. The SFE of nitrite anion estimated by MP2, RI-CCSD(T) and DFT methods with BS-II for two types of solvent model. Values are given in kcal/mol.

Method	PCM	NI-MC-MOZ-SCF
MP2	-65.4	-82.4
RI-CCSD(T)		-83.3
BP86	-65.3	-82.0
CAM-B3LYP	-66.1	-83.2
wB97X-D	-66.7	-83.9
M06	-66.8	-84.1
M06-L	-67.5	-84.9
TPSS	-65.4	-82.3
TPSSh	-66.0	-83.0
Exptl.	-78.8	

$$f_s^{\text{PSE-3}}(\mathbf{r}) = \frac{\Theta\left(-H_s^0(\mathbf{r})\right)}{24} X_s(\mathbf{r})^3, \qquad (7\text{-}1)$$

$$X_s(\mathbf{r}) = -\frac{u_s^0(\mathbf{r})}{k_\mathrm{B}T} + H_s^0(\mathbf{r}) - C_s^0(\mathbf{r}) \qquad (7\text{-}2)$$

where k_B and T denote Boltzmann constant and temperature, respectively. $C_s(\mathbf{r})$ is direct correlation function. $u_s(\mathbf{r})$ represents solute-solvent intermolecular interaction potential and is described as the sum of electrostatic and Lennard-Jones (LJ) potentials. LJ parameters for ruthenium and ligands were taken from Ref. [49] (in Supporting Information) and OPLS[83], respectively as listed in Table 2.

By solving MC-MOZ equation coupled with a closure equation (PSE-3 in this study), $H_s^0(\mathbf{r})$ and $C_s^0(\mathbf{r})$ are obtained. Also, the first derivative of $H_s^0(\mathbf{r})$ with respect to D_{ij}^0 is provided by these coupled equations differentiated by D_{ij}^0. We used 512 (logarithm) radial and 2030 angular (Lebedev) grids to solve MC-MOZ equation. The reference term of direct correlation function was set to zero (method I in Ref. [56]). The residue terms of total and direct correlation functions were expanded with real spherical harmonics up to l = 14. The Obara-Saika recurrence expression[84, 85] was utilized to accelerate the evaluation of electrostatic potential. All the computations concerning the NI-MC-MOZ-SCF method were performed using GAMESS software package[86] modified by us.

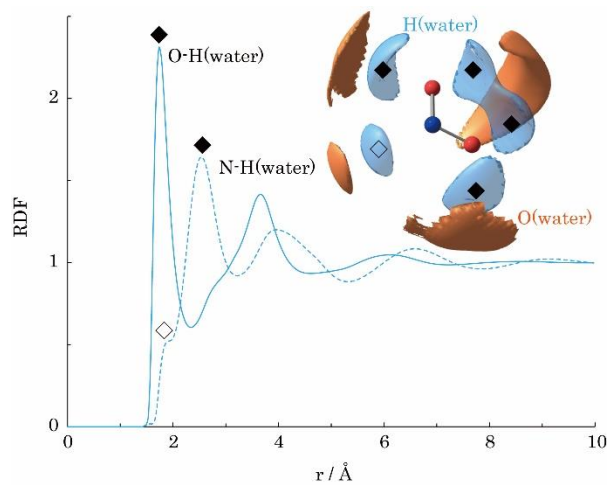

Figure 1. The RDF between free nitrite anion and water hydrogen atom evaluated by CAM-B3LYP/BS-II level of theory using NI-MC-MOZ-SCF method. Blue transparent and orange isosurfaces represent 3D hydrogen and oxygen atom distributions, respectively. The isovalue is 4.0.

The solvent site density pair correlation function was provided by solving the one-dimensional RISM[87–89] coupled with HNC closure. The Temperature of aqueous solution and the number density of solvent are 298.15 K and 0.033426 molecules/Å^3 (= 1.000 g/cm^3), respectively. TIP3P[90]-like model was employed as the solvent water. The LJ parameter of hydrogen atom was modified: the sigma and epsilon are set to 1.000 Å and 0.056 kcal/mol, respectively. This modification was also applied to a hydrogen in solute.

Results and discussion

Before the discussion of complex **A**, **B** and **C**, we check the SFE of free nitrite anion. It is important because there are three or four NO_2 ligands in the complexes and they have a significant large contribution to the SFE of complex, as discussed later. Table 3 lists the SFE estimated by MP2, RI-CCSD(T) and DFT methods with BS-II. In NI-MC-MOZ-SCF, all the methods provide around -83 kcal/mol and show good agreement with the experimental value (-78.8 kcal/mol)[91]. The PCM for all the methods overestimates the observed SFE around 12 kcal/mol because the contributions of

Table 4. MADs of bond lengths and angles in Complex **A** and the N-O stretching frequency of nitrosyl group computed by BP86, CAM-B3LYP, M06 and TPSSh with BS-I. The frequency is already scaled.

Method	MAD		N-O stretching	
	Bond length / Å	Bond angle / degree	Frequency / cm^{-1}	Scaling factor
BP86	0.0381	1.06	1813.3	1.00
CAM-B3LYP	0.0194	1.08	1834.2	0.92
M06	0.0268	0.90	1801.3	0.93
TPSSh	0.0255	1.03	1822.3	0.96
Exptl.			1886	

Table 5. The electronic reorganization energy, excess chemical potential and SFE of complex **A** evaluated by RI-CCSD(T), MP2 and DFT methods with BS-II using NI-MC-MOZ-SCF. Values in parentheses are given by PCM. The unit is kcal/mol.

Method	E^{reorg}		G^{sol}		SFE	
MP2	34.5	(36.8)	-215.5	(-182.2)	-181.0	(-145.4)
RI-CCSD(T)	27.8		-215.5		-187.7	
BP86	7.4	(4.9)	-186.9	(-159.0)	-179.5	(-154.1)
CAM-B3LYP	9.0	(7.0)	-194.8	(-164.0)	-185.7	(-157.0)
ωB97X-D	9.2	(7.1)	-195.5	(-165.3)	-186.3	(-158.2)
M06	8.6	(6.2)	-192.6	(-163.2)	-183.9	(-157.0)
M06-L	7.8	(5.5)	-199.2	(-162.4)	-191.4	(-156.9)
TPSS	7.6	(5.6)	-192.8	(-159.5)	-185.2	(-153.9)
TPSSh	7.9	(5.9)	-187.9	(-161.4)	-180.0	(-155.5)

hydrogen bonds between the anion and water are not adequately incorporated. The E^{gas} and E^{reorg} are provided in Table S1. The zero-point energy is also given in Table S12, including other species. Figure 1 plots the radial distribution function (RDF) between the anion and water hydrogen atom obtained by integrating angular valuables of the 3D hydration structure illustrated in the figure. They are computed at CAM-B3LYP/BS-II level of theory using NI-MC-MOZ-SCF method. Closed and open diamonds show the position corresponding to the RDF peak in the 3D representation. Although it is not clear in the 3D representation, the N-H(water) RDF shows that the hydrogen bond near the nitrogen atom of nitrite anion is very weak and the negatively large SFE comes from hydrogen bonds around the two oxygen atoms.

First, let us discuss complex **A** ($[Ru(NO)(OH)(NO_2)_4]^{2-}$). This compound is isolated as sodium and potassium salt[79]. To select an appropriate optimization method in several DFT functionals, we evaluate the mean absolute deviation (MAD) of bond lengths and angles from the X-ray crystal structure and also compare the frequency of N-O stretching mode of the nitrosyl group (Table 4). The frequency listed in the table is already scaled by the factor determined to reproduce the experimental frequency for NO gas (1876 cm^{-1}). As shown in the table, all the functionals provide a sufficient small MAD and similar frequency. In the functionals, since CAM-B3LYP seems to be slightly better, we employ it as the geometry optimization method in PCM solvent in this study.

In the singlet state of a lot of RuNO complexes, the nitrosyl ligand coordinates the metallic center linearly and the electronic configuration of the $\{RuNO\}^6$ moiety is often considered Ru^{2+}-NO^+ by an electron transfer from the ligand to ruthenium. In practice, in CAM-B3LYP the MOs corresponding to the π^* orbital of NO ligand are vacant, hence, the configuration is considered to be Ru^{2+}-NO^+. Other methods also provide the same result. While several studies already point out that single-determinant DFT gives Ru^{2+}-NO^+ configuration to RuNO complexes, a CASSCF study of *trans*-$[Ru(NO)Cl_4(1H\text{-indazole})]$ with a large active space using the DMRG treatment has reported that the RuNO moiety shows a multiconfigurational nature

and the Ru^{3+}-NO^0 configuration has the largest contribution due to a strong π-back-donation to

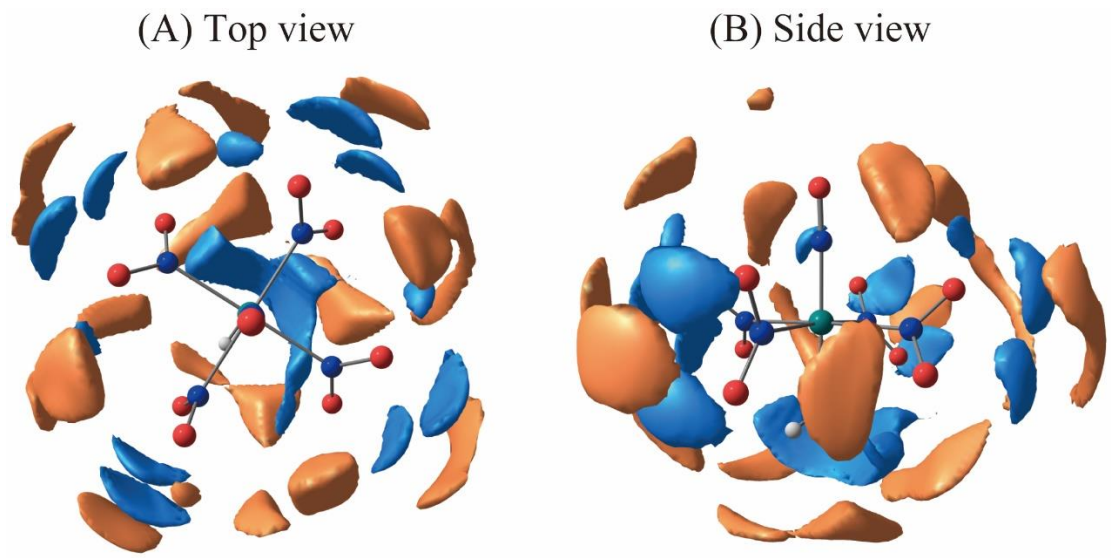

Figure 2. The hydration structure near complex **A** evaluated by MP2/BS-II level of theory using NI-MC-MOZ-SCF method. Blue and orange isosurfaces represent hydrogen (isovalue: 5.0) and oxygen (isovalue: 6.0) atom distributions, respectively.

the NO ligand[10]. But, in this study the error in free energies caused by the multiconfigurational nature may not be sensitive in relative free energies of complex **B** or **C** discussed.

The SFE and hydration structure of complex **A** give a basement in a comparison of those of complex **B** and **C**. The electronic reorganization energy, excess chemical potential and SFE of complex **A** evaluated by RI-CCSD(T), MP2 and DFT methods for two treatments of solvent (PCM and NI-MC-MOZ-SCF) are summarized in Table 5. Different from NO_2^- anion, unfortunately, the experimental data relevant to the SFE have not been reported. In this study, G^{sol} for RI-CCSD(T) is the same as that for MP2 because they are consistent with the density matrix computed at Hartree-Fock (HF) level of theory. In both PCM and NI-MC-MOZ-SCF, the MO method selection does not make a large difference for the SFE evaluation. The SFE by PCM is about -150 kcal/mol and is rather larger than that by NI-MC-MOZ-SCF (less than -180 kcal/mol) due to the difference of G^{sol}. In PCM, the stabilization by hydrogen bonds around the hydroxyl and nitro ligands is not properly estimated. In terms of computational cost, the fact is remarkable that in NI-MC-MOZ-SCF, CAM-B3LYP, ωB97X-D and TPSS have an accuracy comparable with RI-CCSD(T).

To investigate the contribution by each ligand, we decompose $G^{\mathrm{sol},0}$ based on the weight function of MC-MOZ method because G^{sol} decomposition is difficult in the NI-MC-MOZ-SCF formalism. Although here, we use the $G^{\mathrm{sol},0}$ of CAM- B3LYP, the same conclusion is obtained in other cases. The CAM-B3LYP $G^{\mathrm{sol},0}$ is -190.1 kcal/mol and occupies 97.6 % of the G^{sol}. According to the decomposition, the contributions of hydroxyl and four nitro ligands are -26.0 kcal/mol and -175.6 kcal/mol, respectively whereas the nitrosyl ligand has a positive contribution (10.5 kcal/mol). The ruthenium atom contribution (1.0 kcal/mol) is also positive because water does not readily access to it. Figure 2 illustrates the hydration structure near complex **A** evaluated at MP2/BS-II level of theory with NI-MC-MOZ-SCF method. In practice, the hydration

structure is the same as that by HF with BS-II and a similar feature is also given by other methods. The blue isosurface around the hydroxyl and nitro ligands corresponds to hydrogen bonds. They are a source of the large negative contributions to the SFE. Interestingly, the water distribution near the nitro ligands similar to that near a free nitrite anion given in Figure 1. As shown in the panel (A), near the nitrosyl ligand there is no high density area, which is consistent with the positive contribution. A similar trend has been reported in a Monte-Carlo molecular simulation study of $[Ru(NO)(NH_3)_5]^{3+}$ complex in aqueous solution[42, 49]. The hydration structure around the NO ligand might be relevant to the reaction mechanism to convert ruthenium nitrosyl complexes to ruthenium tetroxide in concentrated nitric acid aqueous solution in terms of an easy accessibility of water or reactant to the NO ligand.

Table 6. Calculated bond lengths in Å unit of complex **B** conformers (selected).

Bxyz	Ru−N(NO)	Ru−O(OH)	Ru−N^{ave}(NO$_2$)^a	Ru−O(ONO)
B111	1.766	1.967	2.112(9)	2.112
B112	1.767	1.957	2.111(12)	2.107
B121	1.765	1.957	2.116(9)	2.127
B122	1.766	1.957	2.112(11)	2.106
B211	1.766	1.966	2.120(11)	2.095
B212	1.767	1.958	2.116(15)	2.087
B221	1.765	1.955	2.121(15)	2.113
B222	1.766	1.955	2.117(14)	2.093
B321	1.765	1.960	2.115(15)	2.128

Complex B

Complex **B** is a linkage isomer of complex **A** and one of four NO_2 ligands coordinates the metallic center as nitrito-O ligand. Mentioned above, in this study, nine conformations from **B111** to **B321** are systematically generated.

All the conformers were obtained to have a pseudo-octahedral coordination geometry without any imaginary vibrational frequencies. Table 6 summarizes bond lengths between Ru and donor atoms of the ligands for optimized geometries of complex **B**. The calculated bond lengths for Ru−NO, Ru−OH and Ru−NO_2 are consistent with those of the reference structure, which has 1.761, 1.925 and 2.090 Å, respectively, within the error of 0.032 Å. This shows that all the conformers have a minor-changed geometry of complex **A**. A comparison of the Ru−ligand bond lengths among complex **B** conformers, except Ru−ONO bond lengths, shows almost the same

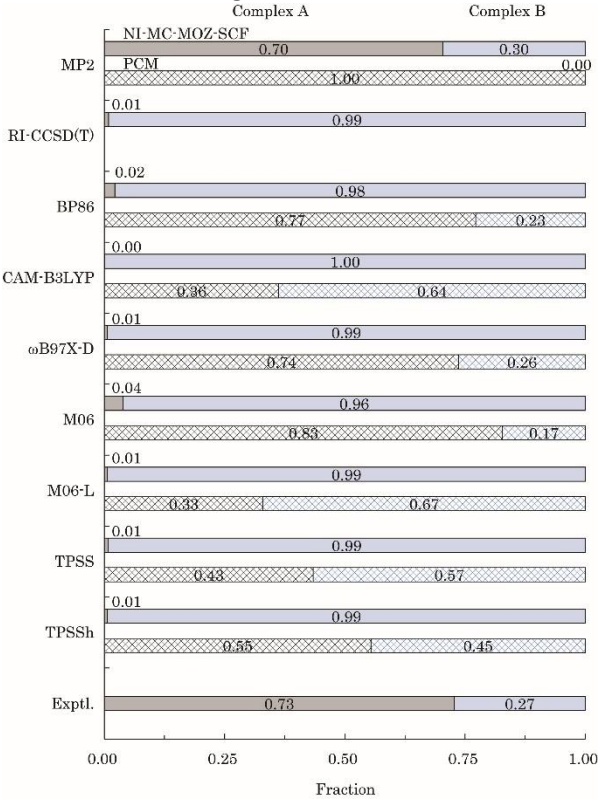

Figure 3. The fraction of complex **A** and **B** in aqueous solution evaluated using free energies of NI-MC-MOZ-SCF and PCM. The experimental value is estimated by the relative ^{15}N NMR signal intensity of the nitrosyl ligand in the complexes.

values each other and the largest deviation was 0.01 Å; whereas, the Ru−ONO bond length varied from 2.09 Å to 2.13 Å and the deviation is larger compared to the other bond lengths.

In all the conformers, the electronic configuration of RuNO moiety is Ru^{2+}-NO^{+}, namely, the isomerisation and conformation change do

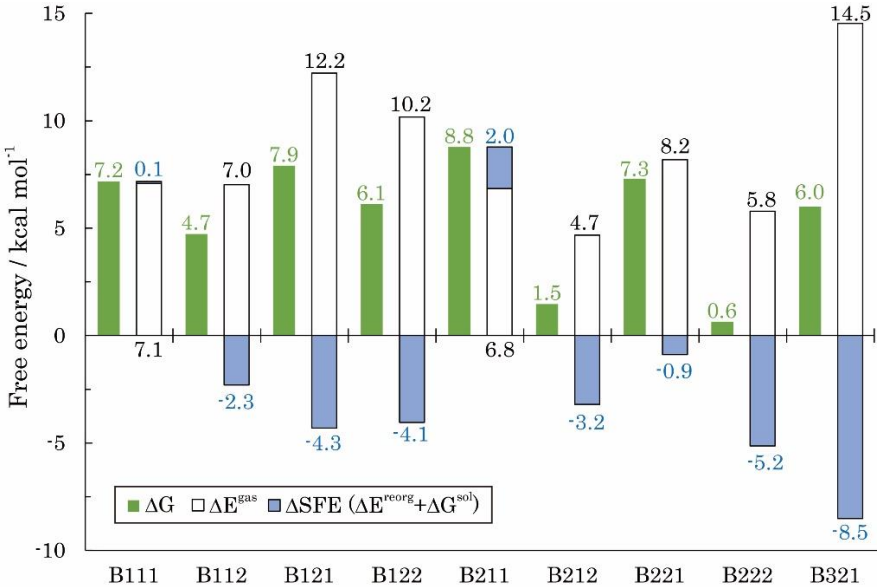

Figure 4. The relative free energy (ΔG) and components (ΔE^{gas} and ΔSFE) of conformers in complex **B** from complex **A** evaluated at MP2/BS-II level of theory with NI-MC-MOZ-SCF.

not make a difference of the electronic configuration of RuNO.

In a few experimental clues for molecular picture of $[RuNO(OH)(NO_2)_4]^{2-}$ and isomers in solution, the fraction of complex **A** and **B** is available by the intensity of ^{15}N NMR signals of the NO ligand[32]. According to the intensity, complex **A** is more stable than complex **B**. The data are useful to find an appropriate method to describe this system. A severe accuracy (~0.1 kcal/mol) is required to reproduce the experimental fraction and the attempt is very challenging. The fraction of complex **A** and **B** in aqueous solution evaluated by their free energy of NI-MC-MOZ-SCF and PCM is presented in Figure 3 with the experimental value. The supporting data are given in Table S3-S7. In the figure, for convenience of explanation, the fractions of nine conformations are added up as complex **B**. In PCM results, the fraction by BP86, ωB97X-D and M06 shows agreement with the experimental value. But, as shown in the figure, the fraction fairly depends on the QM method. In contrast, in NI-MC-MOZ-SCF fractions there is a clear trend that the fraction of complex **B** is much higher than that of complex **A** except for MP2. But, the trend is not consistent with the experiment. Only MP2 provides a similar fraction (complex **A** : **B** = 7 : 3) to the experimental one. Since RI-CCSD(T), of course, is the most reliable QM method in this study, the coincidence by MP2 can result in a balance of errors in the solute energy and SFE evaluations by NI-MC-MOZ-SCF. It is interesting that DFT methods give the same trend as a highly sophisticated one like RI-CCSD(T). Hereafter, we discuss the relative free energy of complex **B** conformers using the MP2 result.

Figure 4 presents the relative free energy of complex **B** conformers from complex **A** (ΔG, green bar) and components (ΔE^{gas} and ΔSFE) evaluated at MP2/BS-II level of theory with NI-MC-MOZ-SCF. All the ΔE^{gas} is positive, which shows that the transformation from nitro coordination to nitrito-

O one is not favorable in $[RuNO(OH)(NO_2)_4]^{2-}$. If solvent is absent (only ΔE^{gas} is considered), **B212** (4.7 kcal/mol) is the most stable and **B222** (5.8 kcal/mol) is the second. In aqueous solution, **B222** provides the smallest ΔG (0.6 kcal/mol) and **B212** does the second (1.5 kcal/mol) due to the cancellation by negative ΔSFE. Since the ΔG of other conformers is more than 4.7 kcal/mol, as a result, **B222** and **B212** are the dominant

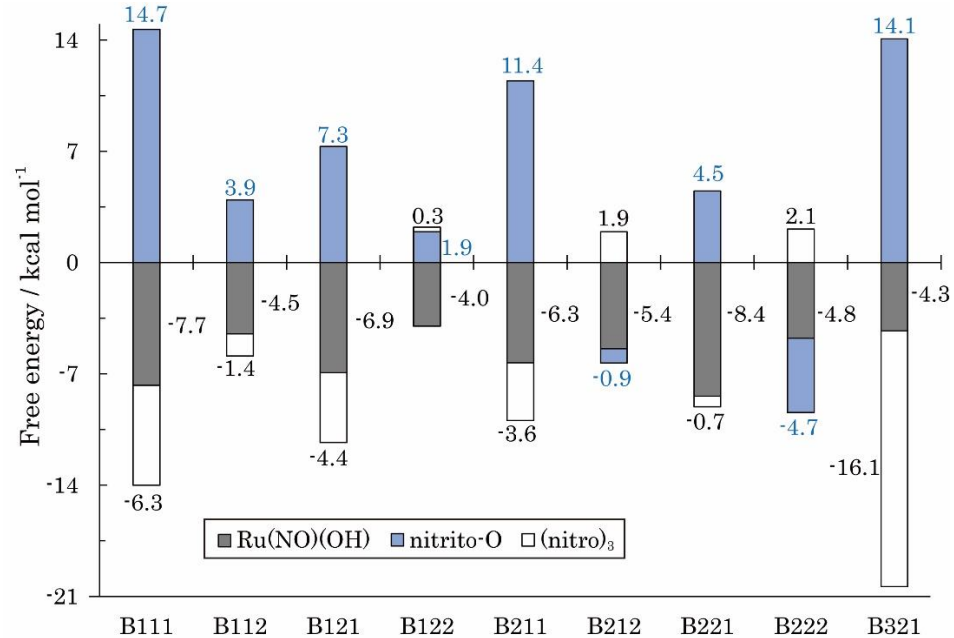

Figure 5. The decomposition of relative $G^{sol,0}$ for complex **B** conformers from complex **A** into the Ru(NO)(OH) moiety, nitrito-O ligand and $(nitro)_3$ moiety evaluated at MP2/BS-II level of theory with NI-MC-MOZ-SCF.

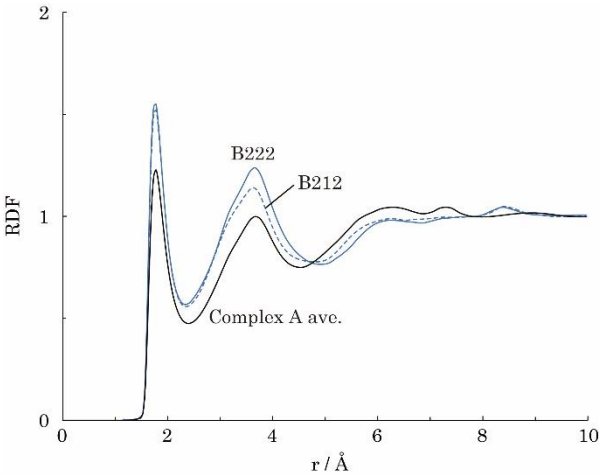

Figure 6. RDFs between H(water) and O(nitrito-O, not bound with ruthenium) of **B212** (blue dashed line) and **B222** (blue solid line) evaluated by MP2/BS-II. For a comparison, the RDF averaged over eight O(nitro)-H(water) ones of complex **A** is also plotted.

conformation in complex **B**. Interestingly, in PCM, **B211** is the most stable in the conformers and it does not depend on the QM method (not shown). Although it is clear that the SFE plays a crucial role to investigate the conformation distribution in aqueous solution, a positively small energy change by the conversion from nitro to nitrito-O in gas phase is primarily important because a large compensation by ΔSFE more than 10 kcal/mol cannot be not expected. Not shown here, the same trend is found in the free energy evaluated by RI-CCSD(T) and DFT methods. All the relative free energy and components are given in Supporting Information (Table S3-S7) as well as the hydration structure (Figure S3-S5).

To understand the SFE change by the conformation of nitrito-O ligand, we decompose $\Delta G^{sol,0}$ into the three contributions; RuNO(OH) moiety, nitrito-O ligand and $(nitro)_3$ moiety.

$\Delta G^{\mathrm{sol},0}$ is applicable to this attempt because SFE is dominated by ΔG^{sol} and $\Delta G^{\mathrm{sol},0}$ occupies more than 95% of ΔG^{sol}. To make the relative value for nitrito-O ligand and $(\mathrm{nitro})_3$ moiety, 1/4 and 3/4 of the $(\mathrm{nitro})_4$ moiety contribution in $G^{\mathrm{sol},0}$ of complex **A** are subtracted, respectively. The decomposition result is given in Figure 5. The RuNO(OH) moiety always provides a negative contribution. Not shown in the figure, it arises from the hydroxyl ligand. Compared with complex

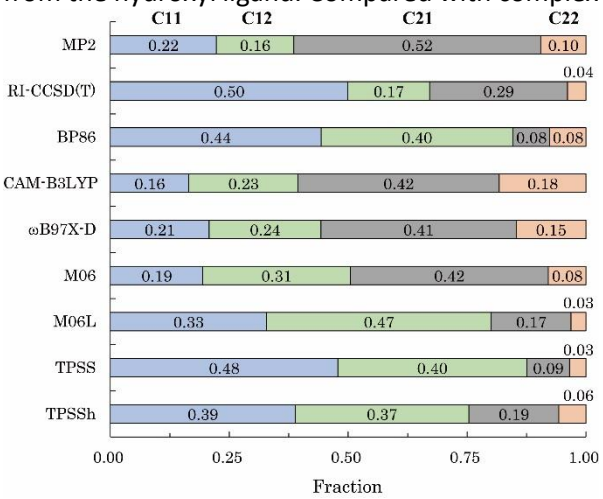

Figure 7. The fraction of complex **C** conformers in aqueous solution evaluated using free energies of NI-MC-MOZ-SCF.

Table 7. The relative free energy (ΔG) and components (ΔE^{gas} and ΔSFE) of conformers in complex **C** evaluated at MP2/BS-II level of theory with NI-MC-MOZ-SCF. Values are given in kcal/mol.

	ΔE^{gas}	ΔSFE	ΔG
C11	0.0	0.0	0.0
C12	5.1	-4.9	0.2
C21	-0.7	0.2	-0.5
C22	3.6	-3.1	0.5

A, in complex **B** conformers, a water molecule to form hydrogen bond is relatively easy to access to the oxygen atom in the hydroxyl ligand. The negative contribution of $(\mathrm{nitro})_3$ moiety except for **B212** and **B222** can be also explained by accessibility of water to nitro ligands near the nitrito-O ligand. The contribution of nitrito-O ligand is expected to be positive because the oxygen atom to form a strong hydrogen bond with water makes a dative bond with ruthenium. In practice, in the conformers except for **B212** and **B222**, the contribution is positive. In **B212** and **B222**, the nitrito-O ligand has a negatively larger $G^{\mathrm{sol},0}$ than the mean of four nitro ligands in complex **A**. It makes them the dominant conformation. Figure 6 plots RDFs between the hydrogen atom of water and oxygen atom of the nitrito-O ligand not bound to ruthenium in **B212** (blue dashed line) and **B222** (blue solid line) evaluated by MP2/BS-II. In this figure, the H(water)-O(nitro) RDF of complex **A** is also plotted for a comparison and is the average over the eight RDFs of complex **A**. In **B212** and **B222**, the first peak in the vicinity of 1.9 Å, which corresponds to the hydrogen bond, is higher than that on the averaged RDF. It is consistent with the decomposition analysis of $G^{\mathrm{sol},0}$.

Complex C

Compared with complex **A**, one of four NO_2 ligands is substituted for aqua one in complex **C**. In this study, mentioned above, four complex **C** conformers are generated by a systematic way (**C11**, **C12**, **C21** and **C22**). Similar to complex **B**, the electron configuration of RuNO moiety in all complex **C** conformers is Ru^{2+}-NO^{+} and does not depend on the MO methods with NI-MC-MOZ-SCF employed in this study.

The structural difference among the conformers is essentially the hydrogen orientation of aqua and hydroxyl ligands. So, the free energy difference among the conformers is expected to be within the thermal fluctuation at room temperature. The fraction of the conformer evaluated using the free energy by NI-MC-MOZ-SCF is given in Figure 7. The E^{gas}, E^{reorg} and G^{sol} are listed in Table S8-S10. Although depending on the method, some of fractions are around 50 %, all the methods give no dominant conformer. A trend is found that **C22** has a small fraction. It, of course, comes from a quite small free-energy difference among the conformers but all the conformers do not have a similar balance between E^{gas} and SFE. The free energy and component of complex **C** conformers evaluated at MP2/BS-II level of theory with NI-MC-MOZ-SCF are listed in Table 7. If solvent is absent,

C11 is more stable by 5.1 kcal/mol than **C12** due to the intramolecular electrostatic interaction between the aqua and hydroxyl ligands in **C11**. But, in aqueous solution, their free energy is comparable because **C12** is stabilized by the hydrogen bond with bulk solvent (Figure S6 and S7). A similar discussion is applicable to **C21** and **C22**.

Stability constant among complex A, B and C

Table 8. The stability constant (K_{ABC} and K'_{ABC}) estimated by MP2 and DFT methods with BS-II using NI-MC-MOZ-SCF.

Method	$\log_{10}K_{\mathrm{ABC}}$	$\log_{10}K'_{\mathrm{ABC}}$
MP2	-17.2	-4.0
BP86	-9.7	-1.7
CAM-B3LYP	-10.3	-0.6
ωB97X-D	-10.5	-0.6
M06	-11.2	-1.6
M06-L	-12.4	-2.3
TPSS	-9.6	-1.7
TPSSh	-10.1	-1.9
Exptl.	-4.5	

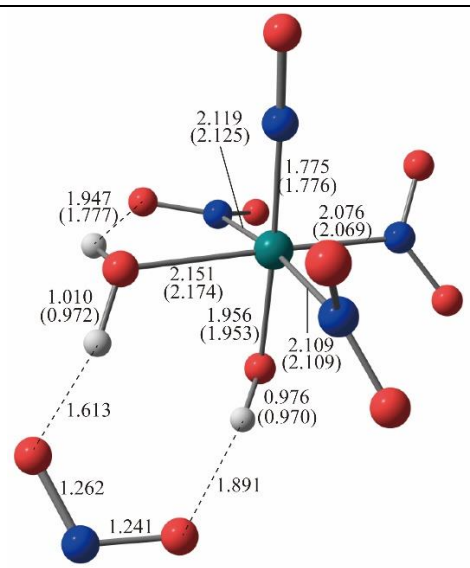

Figure 8. The structure of **C11NO₂** optimized by CAM-B3LYP/BS-I with PCM (water). Bond lengths are given in Å. Values in parentheses correspond to the bond length of **C11**.

Finally, let us discuss the stability constant for the equilibrium among complex **A**, **B** and **C**

$$\mathrm{X} + \mathrm{H_2O} \rightleftharpoons \mathrm{C} + \mathrm{NO_2^-}, \tag{8}$$

where X denotes **A** or **B**. It is fundamental information to quantify a variety of ruthenium nitrosyl complexes in nitric acid aqueous solution with a wide range of the concentration. The experimental value is estimated using the initial concentration of complex **A** and the intensity of ^{15}N NMR signal for the nitrosyl ligand of complex **A**, **B** and **C**[32]. In this study, two types of overall equilibrium constant are defined by taking the contribution from each conformer of complex **B** or **C** into account. The first one (K_{ABC}) is conventional, namely H_2O or NO_2^- are infinitely separated from the complex.

$$K_{\mathrm{ABC}} = \frac{(\sum_i[\mathrm{C}_i])[\mathrm{NO_2^-}]}{([\mathrm{A}] + \sum_i[\mathrm{B}_i])[\mathrm{H_2O}]} = \frac{\sum_i K_{\mathrm{C_{11}C}_i}}{1 + \sum_i K_{\mathrm{AB}_i}} K_{\mathrm{AC_{11}}}, \tag{9-1}$$

$$K_{\mathrm{AB}_i} = \frac{[\mathrm{B}_i]}{[\mathrm{A}]}, \tag{9-2}$$

$$K_{\mathrm{C_{11}C}_i} = \frac{[\mathrm{C}_i]}{[\mathrm{C_{11}}]}, \tag{9-3}$$

$$K_{\mathrm{AC_{11}}} = \frac{[\mathrm{C_{11}}][\mathrm{NO_2^-}]}{[\mathrm{A}][\mathrm{H_2O}]}, \tag{9-4}$$

where the subscript on B or C denotes the conformer. Several studies on ruthenium nitrosyl nitro complexes[46, 48] have reported that a large discrepancy is found between the stability constant evaluated by infinite separation and the experimental value. Similar to the reports, to improve the discrepancy we define an alternative equilibrium constant (K'_{ABC}) by assuming a nitrite-anion-attached **C11** complex (**C11NO₂**, Figure 8), as follows.

$$K'_{\mathrm{ABC}} = \frac{\sum_i K_{\mathrm{C_{11}C}_i}}{1 + \sum_i K_{\mathrm{AB}_i}} K_{\mathrm{AC_{11}NO_2}}, \tag{10-1}$$

$$K_{\mathrm{AC_{11}NO_2}} = \frac{[\mathrm{C_{11NO_2}}]}{[\mathrm{A}][\mathrm{H_2O}]}. \tag{10-2}$$

In $K_{\mathrm{AC_{11}NO_2}}$ calculation, instead of the zero-point energy the free energy correction term is added to consider the entropy loss along the process to yield **C11NO₂**.

Table 8 lists the stability constant (K_{ABC} and K'_{ABC}) estimated by MP2 and DFT methods with BS-II using NI-MC-MOZ-SCF. Unfortunately, we could not perform the RI-CCSD(T) calculation for **C11NO₂** due to the huge computational cost. The E^{gas}, E^{reorg} and G^{sol} of H_2O and **C11NO₂** are listed in Table S2 and S11, respectively. The hydration structure of **C11NO₂** is illustrated in Figure S8. There is a trend that K_{ABC} is negatively much larger than K'_{ABC} and it does not depend on the method,

Table 9. $\Delta G_{\mathrm{C_{11}\text{-}NO_2}}$ decomposition to the gas-phase and SFE terms estimated by MP2 and DFT methods with BS-II using NI-MC-MOZ-SCF. Values are given in kcal/mol.

Method	Gas phase	SFE	$\Delta G_{\mathrm{C_{11}\text{-}NO_2}}$
MP2	45.3	-61.7	-16.4
BP86	48.2	-57.5	-9.2
CAM-B3LYP	47.6	-59.2	-11.6
ωB97X-D	47.1	-59.0	-11.9
M06	46.6	-58.0	-11.4
M06-L	45.8	-58.0	-12.2
TPSS	47.9	-57.0	-9.2
TPSSh	48.2	-57.8	-9.6

which is consistent with previous reports. Similar to the fraction of complex **A** and **B**, K'_{ABC} estimated by MP2 (-4.0) shows good agreement with the experimental value. In the DFT methods, M06-L provides the closest value (-2.3). As shown in Table 9, in MP2, the free energy change for the process

$$\mathrm{C_{11}} + \mathrm{NO_2^-} \overset{\Delta G_{\mathrm{C_{11}\text{-}NO_2}}}{\rightleftharpoons} \mathrm{C_{11NO_2}}, \qquad (11)$$

is negatively large (-16.4 kcal/mol) and smaller than that by DFT methods. Since as illustrated in Figure 8, the **C11** moiety keeps the geometry after the **C11NO₂** formation, the stabilization can be roughly understood by two hydrogen bonds formed between the nitrite anion and **C11**. In particular, the O(nitrite anion)-H(aqua ligand) bond length is very short (1.613 Å) as a hydrogen bond. The energy decomposition provides a nearly constant value to the gas phase and SFE terms, for example, in MP2, the 45.3 kcal/mol and -61.3 kcal/mol, respectively. This is because they are virtually governed by the strong electrostatic potential between **C11** (monovalent anion) and nitrite anion.

Since the experimental value is -4.5, K'_{ABC} presents that an approach that the eliminated nitrite anion interacts with **C11** near it is useful to evaluate a reliable stability constant. This consistency implies that the ligand substitution reaction between NO_2^- and H_2O on complex **A** proceeds via associative interchange pathway. The inert nature in the substitution reaction due to low spin $4d^6$ configuration (t_{2g}^6) of Ru^{2+}-NO^+ octahedral system assures the possibility of a formation of an ion pair or outer-sphere complex[92]. But, it is difficult to discuss in detail that the picture is practical as the ligand exchange process because counter cations are not taken into account in this study. In the experimental condition, complex **A**, **B** and **C** are strongly solvated by counter cations, for example, sodium cation in Ref. [32]. So, the nitrite anion can separate widely from the complex by interacting with the counter cation. To clarify the issue, a simulation on the ligand exchange process is required in the solution system involving the complex, counter cations and solvents.

Conclusions

Ruthenium nitrosyl nitrito-O complex conformers and the stability constant for ligand exchange process in aqueous solution provide a foundation of their behaviours in a more complicated solution system like concentrated nitric acid aqueous solutions and of the transformation to other complex with different ruthenium oxidation number. In this study, $[Ru(NO)(OH)(NO_2)_4]^{2-}$ (complex **A**) and conformers of $[Ru(NO)(OH)(NO_2)_3(ONO)]^{2-}$ (complex **B**) and $[Ru(NO)(OH)(NO_2)_3(H_2O)]^-$ (complex **C**) in aqueous solution have been investigated based on the free-energy calculation by PCM and NI-MC-MOZ-SCF approaches as well as the stability constant among complex **A**, **B** and **C**. The conformation was generated by a systematic way and followed by the geometry optimization with CAM-B3LYP in PCM solvent.

To discuss the accuracy of the relative free energy of complex **B** conformers in aqueous

solution from complex **A** evaluated by PCM and NI-MC-MOZ-SCF, the fraction of complex **A** and **B** was calculated. Whereas in PCM BP86, wB97X-D and M06 provide a similar fraction to that estimated from the intensity of ^{15}N NMR experiment, it fairly depends on the QM method. In NI-MC-MOZ-SCF, there is a trend that complex **B** fraction is much larger than complex **A** except for the MP2 fraction, which is inconsistent with the experiment. These results show that more efforts are required for both PCM and NI-MC-MOZ-SCF to evaluate an accurate free energy of ruthenium nitrosyl nitro or nitrite-O complexes in aqueous solution. Based on the MP2 result by NI-MC-MOZ-SCF, **B222** is dominant in complex **B**. In this study, the MP2 energy was analysed by a decomposition of ΔG and $\Delta G^{\mathrm{sol},0}$. According to the ΔG decomposition, ΔE^{gas} is positive by the conversion from nitro ligand to nitrite-O one and compensated by ΔSFE. A small ΔE^{gas} is important to become the dominant conformer of complex **B** because the ΔSFE compensation is not so negatively large. The $\Delta G^{\mathrm{sol},0}$ analysis shows that the nitro ligand in complex **A** usually obtains more hydration free energy by the hydrogen bond with solvent waters than the nitrite-O ligand.

Two types of the stability constant for the NO_2-aqua ligand exchange process (K_{ABC} and K'_{ABC}) were evaluated by MP2 and DFT methods with NI-MC-MOZ-SCF. For the K'_{ABC} evaluation, a nitrite-anion-attached **C11** (**C11NO$_2$**) was considered. For all the methods, the discrepancy of K'_{ABC} from the experimental value is much smaller than that of K_{ABC}. Similar to the fraction of complex **A** and B, K'_{ABC} by MP2 shows agreement with the experimental value. As also shown in the previous reports, this type of assumption like **C11NO$_2$** is very useful to estimate a reliable stability constant, but it is doubtful as a picture of the ligand exchange process in real aqueous solution due to the absence of counter cations.

As further studies, we attempt to investigate effects of nitric acid concentration on the composition of ruthenium nitrosyl complexes in nitric acid aqueous solution using the original or non-iterative MC-MOZ-SCF by coupling with multi-component RISM. The attempt is toward a proposal of the reaction pathway from the complexes to ruthenium tetroxide in the solution. The mechanism still remains unclear in several decades, which causes uncertainty in evaluation of radioactive ruthenium release during a boiling and dryness of HLLW in the risk assessment of nuclear fuel reprocessing plant.

Acknowledgments

The authors would like to thank Naoki Yoshida (Nuclear Safety Research Center, Japan Atomic Energy Agency (JAEA)) for fruitful discussions and for providing useful experimental data related to this study performed by him and co-workers. Almost computations in the present study have been performed using computational resources provided by Center for Computational Science & e-Systems, JAEA.

Keywords: Ruthenium nitrosyl, hydration structure, molecular-orbital calculation, free energy and multi-center molecular Ornstein-Zernike method

Additional supporting information can be found online in the Supporting Information section at the end of this article.

Data availability statement

The data that supports the findings of this study are available in the supplementary material of this article.

References

[1] Y. Cheng, J.-F. Sun, H.-L. Yang, H.-J. Xu, Y.-Z. Li, X.-T. Chen, Z.-L. Xue, *Organometallics*, **2009**, *28*, 819–823.

[2] E. Fogler, M. A. Iron, J. Zhang, Y. Ben-David, Y. Diskin- Posner, G. Leitus, L. J. Shimon, D. Milstein, *Inorg. Chem.*, **2013**, *52*, 11469–11479.
[3] Y. Liu, S.-M. Ng, S.-M. Yiu, T.-C. Lau, *Dalton Trans.*, **2021**, *50*, 12316–12323.
[4] C. F. Works, P. C. Ford, *J. Am. Chem. Soc.*, **2000**, *122*, 7592–7593.
[5] E. Alessio, G. Mestroni, A. Bergamo, G. Sava, *Curr. Trends Med. Chem.*, **2004**, *4*, 1525–1535.
[6] M. J. Rose, P. K. Mascharak, *Coord. Chem. Rev.*, **2008**, *252*, 2093–2114.
[7] J. H. Enemark, R. D. Feltham, *Coord. Chem. Rev.*, **1974**, *13*, 339–406.
[8] C. G. Hartinger, S. Zorbas-Seifried, M. A. Jakupec, B. Kynast, H. Zorbas, B. K. Keppler, *J. Inorg. Biochem.*, **2006**, *100*, 891–904.
[9] C. G. Hartinger, M. A. Jakupec, S. Zorbas-Seifried, M. Groessl, A. Egger, W. Berger, H. Zorbas, P. J. Dyson, B. K. Keppler, *Chem. Biodiversity*, **2008**, *5*, 2140–2155.
[10] L. Freitag, S. Knecht, S. F. Keller, M. G. Delcey, F. Aquilante, T. Bondo Pedersen, R. Lindh, M. Reiher, L. González, *Phys. Chem. Chem. Phys.*, **2015**, *17*, 14383–14392.
[11] G. Rudstam, *Acta Chem. Scand.*, **1959**, *13*, 1481–1501.
[12] J. M. Fletcher, P. G. M. Brown, E. R. Gardner, C. J. Hardy, A. G. Wain, J. L. Woodhead, *J. Inorg. Nucl. Chem.*, **1959**, *12*, 154–173.
[13] P. G. M. Brown, *J. Inorg. Nucl. Chem.*, **1960**, *13*, 73–83.
[14] D. Scargill, C. E. Lyon, N. R. Large, J. M. Fletcher, *J. Inorg. Nucl. Chem.*, **1965**, *27*, 161–171.
[15] J. M. Fletcher, C. E. Lyon, A. G. Wain, *J. Inorg. Nucl. Chem.*, **1965**, *27*, 1841–1851.
[16] G. G. J. Boswell, S. Soentono, *J. Inorg. Nucl. Chem.*, **1981**, *43*, 1625–1632.
[17] A. Siczek, M. Steindler, *At. Energy Rev.*, **1978**, *16*, 575–618.
[18] D. Pruett, *Radiochim. Acta*, **1980**, *27*, 115–120.
[19] P. Swain, C. Mallika, R. Srinivasan, U. K. Mudali, R. Natarajan, *J. Radioanal. Nucl. Chem.*, **2013**, *298*, 781–796.
[20] S. R. Reddy, R. Trikha, R. Murali, E. Augustine, N. Desigan, N. K. Pandey, C. Mallika, U. K. Mudali, J. B. Joshi, *Prog. Nucl. Energy*, **2016**, *86*, 50–62.
[21] C. Lefebvre, T. Dumas, M. Charbonnel, P. Solari, *Procedia Chem.*, **2016**, *21*, 54–60.
[22] P. Moeyaert, M. Miguirditchian, M. Masson, B. Dinh, X. Hérès, S. De Sio, C. Sorel, *Chem. Eng. Sci.*, **2017**, *158*, 580–586.
[23] C. Lefebvre, T. Dumas, C. Tamain, T. Ducres, P. L. Solari, M.-C. Charbonnel, *Ind. Eng. Chem. Res.*, **2017**, *56*, 11292–11301.
[24] P. K. Verma, P. K. Mohapatra, *Sep. Purif. Technol.*, **2021**, *275*, 119148.
[25] A. Sasahira, F. Kawamura, *J. Nucl. Sci. Technol.*, **1988**, *25*, 472–478.
[26] A. Sasahira, F. Kawamura, *J. Nucl. Sci. Technol.*, **1988**, *25*, 603–606.
[27] H. Igarashi, K. Kato, T. Takahashi, *Radiochim. Acta*, **1993**, *60*, 143–148.
[28] C. Mun, L. Cantrel, C. Madic, *Nucl. Technol.*, **2006**, *156*, 332–346.
[29] N. Yoshida, T. Ohno, Y. Amano, H. Abe, *J. Nucl. Sci. Technol.*, **2018**, *55*, 599–604.
[30] N. Yoshida, T. Ono, R. Yoshida, Y. Amano, H. Abe, *J. Nucl. Sci. Technol.*, **2020**, *57*, 1–9.
[31] V. Emel'yanov, M. Fedotov, *Russ. J. Inorg. Chem.*, **2006**, *51*, 1811–1819.
[32] E. V. Kabin, V. A. Emel'yanov, S. V. Tkachev, *Russ. J. Inorg. Chem.*, **2013**, *58*, 229–238.
[33] T. Dirks, T. Dumas, D. Guillaumont, M.-C. Charbonnel, *J. Radioanal. Nucl. Chem.*, **2020**, *326*, 1213–1223.
[34] J. Gao, D. G. Truhlar, *Annu. Rev. Phys. Chem.*, **2002**, *53*, 467–505.
[35] H. Lin, D. G. Truhlar, *Theor. Chem. Acc.*, **2007**, *117*, 185.
[36] B. F. Straub, *Angew. Chem. Int. Ed.*, **2005**, *44*, 5974–5978.
[37] G. F. Caramori, G. Frenking, *Organometallics*, **2007**, *26*, 5815–5825.
[38] G. F. Caramori, A. G. Kunitz, K. F. Andriani, F. G. Doro, G. Frenking, E. Tfouni, *Dalton Trans.*, **2012**, *41*, 7327–7339.

[39] C. M. Aguilar, W. R. Rocha, *Inorg. Chim. Acta*, **2013**, *408*, 18–26.
[40] L. Freitag, L. González, *Inorg. Chem.*, **2014**, *53*, 6415–6426.
[41] K. Andriani, G. Caramori, A. Muñoz-Castro, F. Doro, *RSC Advances*, **2015**, *5*, 69057–69066.
[42] G. L. Rodrigues, W. R. Rocha, *J. Phys. Chem. B*, **2016**, *120*, 11821–11833.
[43] A. P. de Lima Batista, A. G. de Oliveira-Filho, S. E. Galembeck, *Phys. Chem. Chem. Phys.*, **2017**, *19*, 13860–13867.
[44] J. Sanz Garcıa, F. Talotta, F. Alary, I. M. Dixon, J.-L. Heully, M. Boggio-Pasqua, *Molecules*, **2017**, *22*, 1667.
[45] F. Talotta, J.-L. Heully, F. Alary, I. M. Dixon, L. González, M. Boggio-Pasqua, *J. Chem. Theory Comput.*, **2017**, *13*, 6120–6130.
[46] M. Kaneko, A. Kato, S. Nakashima, Y. Kitatsuji, *Inorg. Chem.*, **2019**, *58*, 14024–14033.
[47] F. Talotta, L. González, M. Boggio-Pasqua, *Molecules*, **2020**, *25*, 2613.
[48] A. Kato, M. Kaneko, S. Nakashima, *RSC advances*, **2020**, *10*, 24434–24443.
[49] G. L. Silva Rodrigues, W. R. Rocha, *Int. J. Quant. Chem.*, **2021**, *121*, e26476.
[50] J. Tomasi, B. Mennucci, R. Cammi, *Chem. Rev.*, **2005**, *105*, 2999–3094.
[51] B. Mennucci, *Wiley Interdiscip. Rev.: Comput. Mol. Sci.*, **2012**, *2*, 386–404.
[52] K. Kido, K. Kasahara, D. Yokogawa, H. Sato, *J. Chem. Phys.*, **2015**, *143*, 014103.
[53] K. Kido, *J. Comput. Chem.*, **2019**, *40*, 2072–2085.
[54] D. Yokogawa, H. Sato, S. Sakaki, *J. Mol. Liq.*, **2009**, *147*, 112–116.
[55] D. Yokogawa, H. Sato, T. Imai, S. Sakaki, *J. Chem. Phys.*, **2009**, *130*, 064111.
[56] K. Kido, D. Yokogawa, H. Sato, *Chem. Phys. Lett.*, **2012**, *531*, 223–228.
[57] J.-P. Hansen, I. R. McDonald, in Theory of simple liquids; Elsevier,Amsterdam, **1990**.
[58] F. Hirata, in Molecular theory of solvation; Kluwer Academic, Dordrecht, **2003**; Vol. 24.
[59] J. J. Howard, B. M. Pettitt, *J. Stat. Phys.*, **2011**, *145*, 441–466.
[60] H. Sato, *Phys. Chem. Chem. Phys.*, **2013**, *15*, 7450–7465.
[61] T. Morita, K. Hiroike, *Prog. Theor. Phys.*, **1960**, *23*, 1003–1027.
[62] S. J. Singer, D. Chandler, *Mol. Phys.*, **1985**, *55*, 621–625.
[63] K. Kido, D. Yokogawa, H. Sato, *J. Chem. Phys.*, **2012**, *137*, 024106.
[64] A. D. Becke, *Phys. Rev. A*, **1988**, *38*, 3098.
[65] J. P. Perdew, *Phys. Rev. B*, **1986**, *33*, 8822.
[66] T. Yanai, D. P. Tew, N. C. Handy, *Chem. Phys. Lett.*, **2004**, *393*, 51–57.
[67] Y. Zhao, D. G. Truhlar, *Theor. Chem. Acc.*, **2008**, *120*, 215–241.
[68] J. Tao, J. P. Perdew, V. N. Staroverov, G. E. Scuseria, *Phys. Rev. Lett.*, **2003**, *91*, 146401.
[69] J. P. Perdew, J. Tao, V. N. Staroverov, G. E. Scuseria, *J. Chem. Phys.*, **2004**, *120*, 6898–6911.
[70] Gaussian 16, Revision C.01, M. J. Frisch, G. W. Trucks, H. B. Schlegel, G. E. Scuseria, M. A. Robb, J. R. Cheeseman, G. Scalmani, V. Barone, G. A. Petersson, H. Nakatsuji, X. Li, M. Caricato, A. V. Marenich, J. Bloino, B. G. Janesko, R. Gomperts, B. Mennucci, H. P. Hratchian, J. V. Ortiz, A. F. Izmaylov, J. L. Sonnenberg, D. Williams-Young, F. Ding, F. Lipparini, F. Egidi, J. Goings, B. Peng, A. Petrone, T. Henderson, D. Ranasinghe, V. G. Zakrzewski, J. Gao, N. Rega, G. Zheng, W. Liang, M. Hada, M. Ehara, K. Toyota, R. Fukuda, J. Hasegawa, M. Ishida, T. Nakajima, Y. Honda, O. Kitao, H. Nakai, T. Vreven, K. Throssell, J. A. Jr. Montgomery, J. E. Peralta, F. Ogliaro, M. J. Bearpark, J. J. Heyd, E. N. Brothers, K. N. Kudin, V. N. Staroverov, T. A. Keith, R. Kobayashi, J. Normand, K. Raghavachari, A. P. Rendell, J. C. Burant, S. S. Iyengar, J. Tomasi, M. Cossi, J. M. Millam, M. Klene, C. Adamo, R. Cammi, J. W. Ochterski, R. L. Martin, K. Morokuma, O. Farkas, J. B. Foresman, D. J. Fox, Gaussian, Inc., Wallingford CT, 2016.
[71] D. Datta, M. S. Gordon, *J. Chem. Theory Comput.*, **2021**, *17*, 4799–4822.
[72] J.-D. Chai, M. Head-Gordon, *Phys. Chem. Chem. Phys.*, **2008**, *10*, 6615–6620.

[73] J. G. Hill, J. A. Platts, *J. Chem. Phys.*, **2008**, *129*, 134101.
[74] P. J. Hay, W. R. Wadt, *J. Chem. Phys.*, **1985**, *82*, 299–310.
[75] T. H. Dunning Jr, *J. Chem. Phys.*, **1989**, *90*, 1007–1023.
[76] R. A. Kendall, T. H. Dunning Jr, R. J. Harrison, *J. Chem. Phys.*, **1992**, *96*, 6796–6806.
[77] A. Ehlers, M. Böhme, S. Dapprich, A. Gobbi, A. Höllwarth, V. Jonas, K. Köhler, R. Stegmann, A. Veldkamp, G. Frenking, *Chem. Phys. Lett.*, **1993**, *208*, 111–114.
[78] L. E. Roy, P. J. Hay, R. L. Martin, *J. Chem. Theory Comput.*, **2008**, *4*, 1029–1031.
[79] V. Emel'yanov, I. Baidina, S. Gromilov, A. Virovets, *J. Struct. Chem.*, **2006**, *47*, 63–70.
[80] A. V. Marenich, C. J. Cramer, D. G. Truhlar, *J. Phys. Chem. B*, **2009**, *113*, 6378–6396.
[81] D. Yokogawa, H. Sato, S. Sakaki, *J. Chem. Phys.*, **2007**, *126*, 244504.
[82] S. M. Kast, T. Kloss, *J. Chem. Phys.*, **2008**, *129*, 236101.
[83] W. L. Jorgensen, D. S. Maxwell, J. Tirado-Rives, *J. Am. Chem. Soc.*, **1996**, *118*, 11225–11236.
[84] S. Obara, A. Saika, *J. Chem. Phys.*, **1986**, *84*, 3963–3974.
[85] S. Obara, A. Saika, *J. Chem. Phys.*, **1988**, *89*, 1540–1559.
[86] M. W. Schmidt, K. K. Baldridge, J. A. Boatz, S. T. Elbert, M. S. Gordon, J. H. Jensen, S. Koseki, N. Matsunaga, K. A. Nguyen, S. Su, T. L. Windus, M. Dupuis, J. A. Montgomery, *J. Comput. Chem.*, **1993**, *14*, 1347–1363.
[87] D. Chandler, H. C. Andersen, *J. Chem. Phys.*, **1972**, *57*, 1930–1937.
[88] F. Hirata, P. J. Rossky, *Chem. Phys. Lett.*, **1981**, *83*, 329–334.
[89] F. Hirata, P. J. Rossky, B. M. Pettitt, *J. Chem. Phys.*, **1983**, *78*, 4133–4144.
[90] W. L. Jorgensen, J. Chandrasekhar, J. D. Madura, R. W. Impey, M. L. Klein, *J. Chem. Phys.*, **1983**, *79*, 926–935.
[91] Y. Marcus, *J. Chem. Soc., Faraday Trans.*, **1991**, *87*, 2995–2999.
[92] F. Basolo, R. G. Pearson, in Mechanisms of inorganic reactions: Study of metal complexes in solution, 2nd ed., John Wiley and Sons, Inc., New York, **1967**; Chapter 3.

GRAPHICAL ABSTRACT

Kentaro Kido and Masashi Kaneko

TITLE: Conformation, hydration and ligand exchange process of ruthenium nitrosyl complexes in aqueous solution: Free-energy calculations by a combination of MO theories and different solvent models

ABSTRACT: Conformation, hydration and ligand exchange process of several ruthenium nitrosyl complexes are investigated using a combination approach of molecular-orbital theories and a state-of-the-art molecular solvation technique. Thanks to the solvent model, solvation free energy is readily computed from the hydration structure. Interestingly, the dominant conformation is different between the approach and widely-used polarizable continuum solvent model. In the ligand substitution reaction between NO_2^- and H_2O, proceeding via associative interchange pathway is supported.

GRAPHICAL ABSTRACT FIGURE